Archives of Materials Science and Engineering

Volume 90
Issue 1
March 2018
Pages 16-24

International Scientific Journal
published monthly by the
World Academy of Materials
and Manufacturing Engineering

The impact of nozzle configuration on the heat transfer coefficient

K. Krupanek *, A. Staszczyk, J. Sawicki, P. Byczkowska
Institute of Materials Science and Engineering, Lodz University of Technology,
ul. Stefanowskiego 1,15, 90-924 Łódź, Poland
* Corresponding e-mail address: krzysztof.krupanek@p.lodz.pl

ABSTRACT

Purpose: The purpose of this paper is to elaborate guidelines regarding geometric configurations of a nozzle manifold that have an impact on the effectiveness of the quenching process and occurrence of quenching distortions.

Design/methodology/approach: Within the framework of this study there an optimisation of nozzle manifold geometry was carried out with the help of numerical simulations created using Ansys CFX software. In the first stage, a simplification of the nozzle-sample system reduced to a two-dimensional simulation was employed to determine the most optimal location of the coolant stream. In the second stage, several arrangements of nozzle manifolds were tested in a three-dimensional simulation. The parameters that were taken into account included the rate of sample cooling, the uniformity of cooling with a sample volume and heat coefficient takeover read from its surface.

Findings: The different active/inactive nozzle arrangements within the manifold and the impact of the specific arrangements on the uniformity of heat transfer from the sample surface were compared.

Research limitations/implications: The simulations carried out within the framework of this study are one of the elaboration stages of a new flow heat treatment technology.

Practical implications: The application of an efficient cooling chamber in flow treatment makes it possible to limit quenching distortions to a minimum. An optimal adjustment of cooling parameters and cooling nozzle configuration to the shape of the element in order to make the cooling uniform translate directly into a reduction in distortions. Avoiding the necessity to reduce distortions after quenching means there is a significant reduction in detail production costs (grinding).

Originality/value: The concept of single-piece flow in the heat treatment for the mass industry is developing rapidly and constitutes a fully automated element of a manufacturing line, adjusted for the purposes of being included in the production process automatic control system. It also makes it possible to conduct comprehensive and integration quality supervision and management at the level of an individual element, which is not possible in the case of batch heat treatment, which is a gap in the production process.

Keywords: High-pressure gas quenching, Heat treatment, Case hardening, Nozzle manifold, Flow simulation, CFX

Reference to this paper should be given in the following way:

K. Krupanek, A. Staszczyk, J. Sawicki, P. Byczkowska, The impact of nozzle configuration on the heat transfer coefficient, Archives of Materials Science and Engineering 90/1 (2018) 16-24.

METHODOLOGY OF RESEARCH, ANALYSIS AND MODELLING

1. Introduction

The efficient cooling of elements subjected to the quenching process is of key importance regarding achieving the product quality expected. Non-uniform cooling of batch volume leads to the occurrence of quenching distortions [1-3], which have to be removed later by means of subtractive processing, e.g., through grinding [4]. From the point of view of mass production, this is very costly and undesirable [5-7].

The task of the modern quenching systems is to ensure uniform inflow of cooling gas from all directions around the additionally rotating detail. The correction of quenching distortions is one of the most expensive processes. In order to limit the occurrence of such distortions, there are elaborate advanced cooling systems where the details are processed individually, and the gas is used as the cooling medium [8-12].

A stream of liquid hitting the element surface can take over energy from it very effectively in the form of heat [13]. The simulation of behavior and efficiency of a stream of liquid within the material cooling process is the subject of many authors' deliberations. It has been proved that in the area of stagnation of the gas stream hitting the material surface at a right angle good heat transfer parameters have resulted [14]. Such solutions are applied not only in the quenching process, but also in the efficient cooling of electronic systems or, for example, in the paper and textile manufacturing process [15]. The distance of the stream from the surface of the element cooled is very significant for the heat permeation efficiency, which is confirmed by both simulations and experiment results [16]. Studies exist that show the impact of the shape and dimension of a single nozzle on the heat flow [17]. There is also a correlation between the heat flow value and the turbulence intensity within a given system [18]. Some of the authors focused specifically on studying heat flow in cases where the temperature difference between the liquid and the sample is large [19-21], even as high as 700°C [22], which is close to the conditions prevalent in a quenching chamber.

Next, to the impact of individual nozzles, the behavior of dual-nozzle systems has also been studied [23]. In such a system, the streams of a liquid interact with one another, which may lead to the formation of the so-called secondary stagnation zones. Many different shapes of the nozzle manifold layout have been studied [24,25].

Numerous reports from the literature prove that numerical simulations of gas flow and sample cooling can constitute a reliable instrument used for optimising the nozzle manifold geometry in order to achieve the best possible efficiency and uniformity of cooling.

2. Description of methodology

2.1. Single nozzle 2D geometric model

The model of the nozzle-sample system consisted of a single nozzle directed towards the sample at a right angle (Fig. 1).

The Reynolds number in the nozzle and distance from the nozzle outlet to the sample were changed in order to test all the possible configurations thereof.

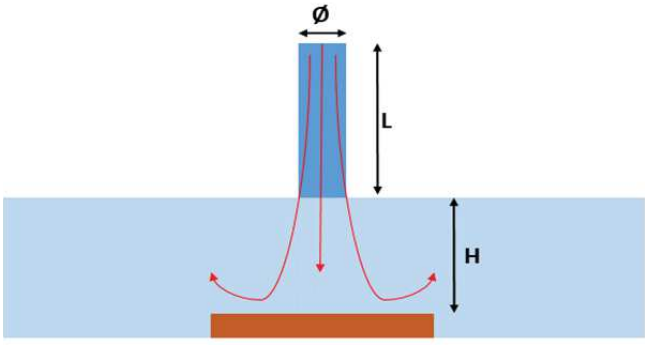

Fig. 1. Geometry of the model

Changing parameters:

- Re: 11000, 22000, 44000;
- H/D: 1, 2, 3, 4, 5,6.

The simplification of the simulation down to two dimensions at the first stage of calculations is aimed at comparing different geometries and determining the right direction for designing an appropriate manifold.

2.2. Double nozzle 3D geometric model

Double nozzle configuration a 3D model was simulated for changing geometrical parameters (Figs. 2,3). The model configurations were simulated for one nozzle entrance speed.

It was assumed that the flow is more or less symmetrical in relation to the plane that cuts both nozzles in half.

Changing parameters:

- S/D: 1, 2, 3, 4;
- H/D: 1, 2, 3, 4, 5,6.

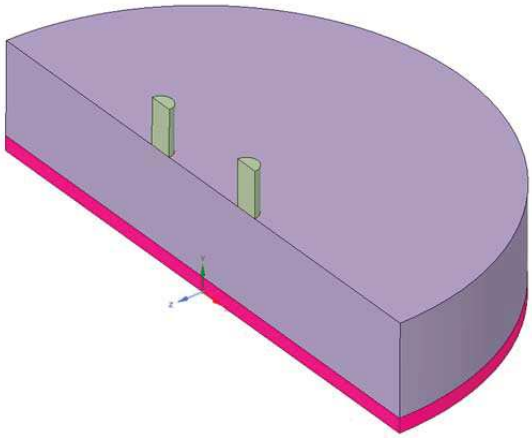

Fig. 2. Geometry of the 3D model

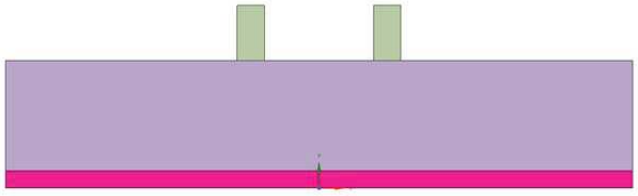

Fig. 3. Geometry of the 3D model

2.3. Boundary conditions

The model present in Figure 1 was simulated in Ansys CFX solver for computational fluid dynamics. The following boundary conditions were adopted:

Chamber:

- Gas – nitrogen, ideal gas;
- Radiation – Surface to Surface model.

Turbulence model

When RANS turbulence model is properly adapted to a given flow, it can adequately predict the impact of small scales structures on the mean flow parameters and calculate reasonable time-averaged results.

In this work, the shear stress transport (SST) model by Menter was applied. SST model combines the best of two models: "k-ω" and "k-ε" The k-ω formulation is used in the viscous sub-layer of the boundary layer. In outer layers from the wall in the free stream region model switches to a k-ε behavior so that it avoids the common k-ω problem that the model is too sensitive to the inlet free-stream turbulence properties.

Turbulence Kinetic Energy:

$$\frac{\partial(\rho k)}{\partial t}+\frac{\partial(\rho \mathrm{u}_j k)}{\partial x_j}=-P-\beta^*\rho\omega k\ +\frac{\partial}{\partial x_j}\left[\frac{(\mu+\sigma_k\mu_t)\partial k}{\partial x_j}\right] \tag{1}$$

Specific Dissipation Rate:

$$\frac{\partial(\rho\omega)}{\partial t}+\frac{\partial(\rho \mathrm{u}_j\omega)}{\partial x_j}=-\frac{\gamma}{\upsilon_t}P-\beta^*\rho\omega^{\,2}+\frac{\partial}{\partial x_j}\Big[(\mu+\sigma_\omega\mu_t)\frac{\partial\omega}{\partial x_j}\Big]+2(1-F_1)\frac{\rho\sigma_{\omega2}}{\partial\omega}\frac{\partial k}{\partial x_j}\frac{\partial\omega}{\partial x_j} \tag{2}$$

where Kinematic Eddy Viscosity:

$$\upsilon_t=\frac{a_1 k}{\max(a_1\omega,SF_2)} \tag{3}$$

Production term:

$$P=-\mu_t SS \tag{4}$$

where:

$$S=\sqrt{\frac{1}{2}\left(\frac{\partial \mathrm{u}_i}{\partial x_j}+\frac{\partial \mathrm{u}_j}{\partial x_i}\right)^2} \tag{5}$$

Production term modification

The Kato and Launder modification were applied. The Standard SST turbulence model tends to overpredict turbulent production term in stagnation regions term because of high values of S that are calculated in those regions. Thus heat transfer is as well influence by this overprediction. The proposal by Kato and Launder is to replace one of the strain-rates, S, in the turbulent production term with the vorticity, Ω. The Kato-Launder modified production then becomes:

$$P=\mu_t S\Omega \tag{6}$$

where:

$$\Omega=\sqrt{\frac{1}{2}\left(\frac{\partial \mathrm{u}_i}{\partial x_j}+\frac{\partial \mathrm{u}_j}{\partial x_i}\right)^2} \tag{7}$$

In conjunction with nearly irrotational deformation in the stagnation region, the value of **Ω** is close to zero. This causes a reduction of the turbulence production. In a simple shear flow, the modification has no effects.

Nozzle inlet:

- Velocity values were calculated for the assumed Reynolds numbers:

- Single nozzle: 11000, 22000, 44000,
- Double nozzle: 22000,
- Inlet turbulence intensity 10%.

Outlet:
- Relative pressure: 0 bar,
- Condition: Opening.

Chamber walls:
- Condition: No slip wall,
- Radiation activated.

The contact surface between the sample and the liquid chamber:
- Interface with heat flow.

Bottom of the sample and the chamber:
- Symmetry assumed.

Starting conditions of the simulation:
- The gas temperature in the chamber is set to 20°C,
- The initial sample temperature is set to 850°C.

2.4. Computational mesh of the models

The computational mesh was created using Ansys Mesh software. In the area of the nozzles and over the sample cooled there a structural mesh consisting of hexahedral elements was created, while the remaining part of the liquid domains was filled with tetrahedral elements. Using an inflation layer, the mesh was densified in the wall-side layer of the nozzles and the sample in order to receive the "y+" parameter lower than or equal to 1 (Figs. 4,5). In simulations with convective heat transfer, in order to obtain reliable results, it is crucial to creating a high-quality mesh in the boundary layer and stagnation regions.

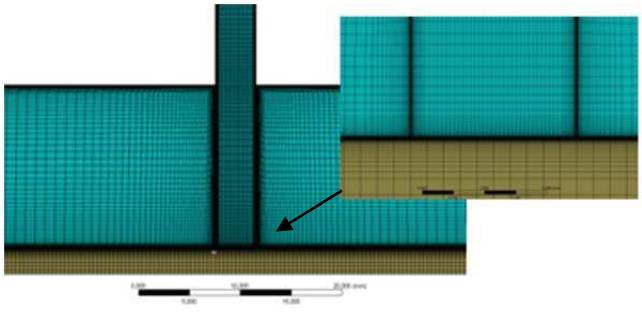

Fig. 4. Discrete model of the 2D nozzle, the sample, and space between them

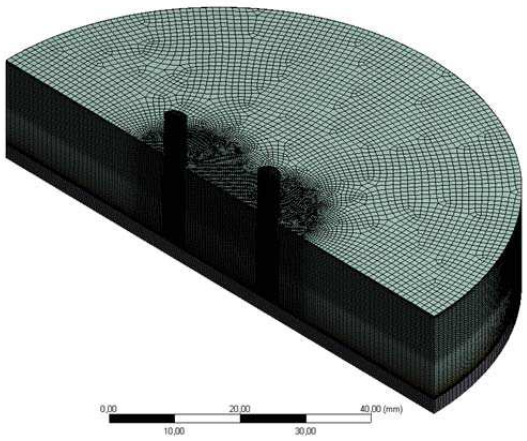

Fig. 5. Discrete model of the 3D double nozzle, the sample, and space between them

3. Results

The parameters measured during the simulation that were compared are:

- Convective heat transfer coefficient α, averaged for the top surface of the sample cooled and maximum value The α was determined on the basis of the following formula:

$$\alpha = \frac{q}{\Delta T} \quad \left[\frac{W}{m^2 \cdot K}\right] \tag{8}$$

where: q – heat flux, T_w – temperature on the sample surface, T_{out} – the temperature of the gas in the chamber;

- Reynolds number:

$$Re = \frac{\rho \cdot u \cdot l}{\mu} \tag{9}$$

where: ρ – density, u –mean velocity, l- characteristic length, μ – dynamic viscosity;

- Nusselt number is the ratio of convective to conductive heat transfer across the boundary. When it is close to one, it means that heat convection has a similar magnitude to heat conduction in the fluid. For high Reynolds flows Nu can range between 100:1000.

$$Nu = \frac{\alpha \cdot l}{\lambda} \tag{10}$$

where: α – Convective heat transfer coefficient, l – characteristic length, λ – thermal conductivity of the fluid.

3.1. Results of 2D simulation

The profile of velocity in the nozzle and at its outlet depends on the geometry thereof. As a result of the impact of the viscous forces in the wall-side layer, in cylindrical nozzles, a parabolic velocity profile characteristic of flows inside pipes is formed. Next, depending on the distance from the surface cooled, the gas stream flowing out of the nozzle may create a free flow zone. In that zone, the outflowing stream transfers on its limits, through viscous forces, the momentum to gas particles located in the chamber and slows down at the same time, narrowing the velocity profile and dragging additional liquid particles, thus increasing the mass flow – Fig. 6.

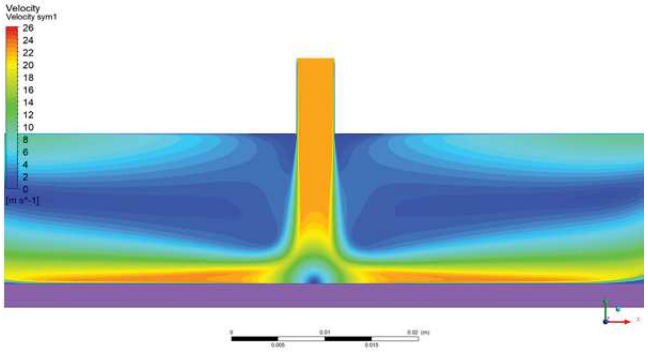

Fig. 6. Distribution of gas velocities in the 2D model

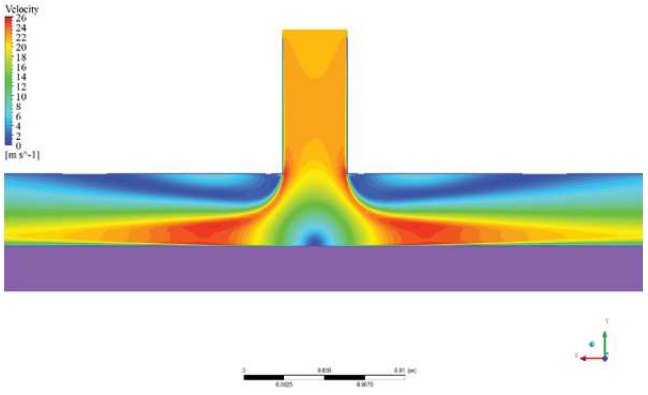

Fig. 7. Distribution of gas velocities in the 2D model, nozzle located near the wall

When the nozzle outlet is located near the sample, the stagnation zone influences the formation of the flow after it leaves the nozzle, creating high velocity flows on both sides of stagnation region – Figs. 7,8. Then the flow hits the cooled surface, losing the velocity component perpendicular to it thereby creating a high static pressure zone. This zone is called the stagnation zone, where high velocity and pressure gradients occur. Due to the sudden change in the inflow direction and the high velocity and pressure gradients present, shear stress and normal stress appear in the liquid that improve the local parameters of heat transfer in gas. Next, the gas leaves the stagnation zone as a result of expansion and accelerates in the direction parallel to the surface, flowing around it uniformly. In perpendicular cooling with a single nozzle, there are 2 zones of increased heat transfer present: in the stagnation zone and the zone where the flow achieves the maximum velocity over the sample surface.

The results obtained after 2D simulations showed that the nozzle Reynolds number is the most important parameter. Figure 9 shows that the biggest average heat transfer values were achieved for the Re= 44000. In each flow, the best values occur at a distance to the nozzle diameter correlation equal to 1. Figures 10, 11 and 12 show the same tendency for the maximum Nusselt number.

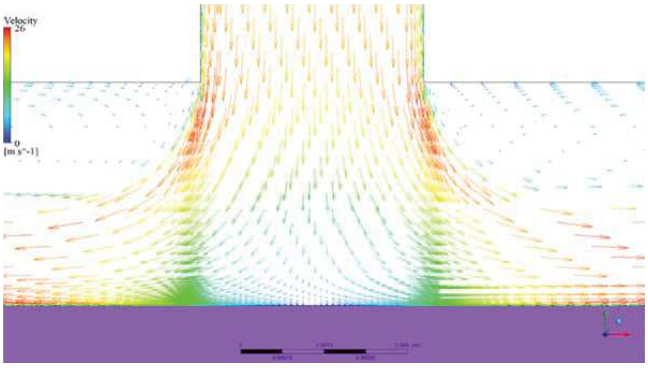

Fig. 8. Velocity vector field in the 2D model, nozzle located near the wall

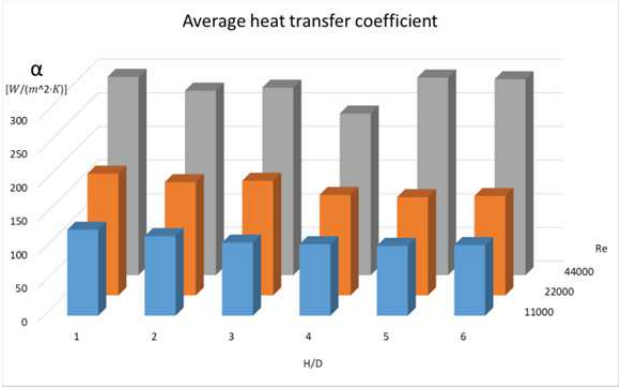

Fig. 9. Graph of heat transfer coefficient for different distances between the nozzle and the sample

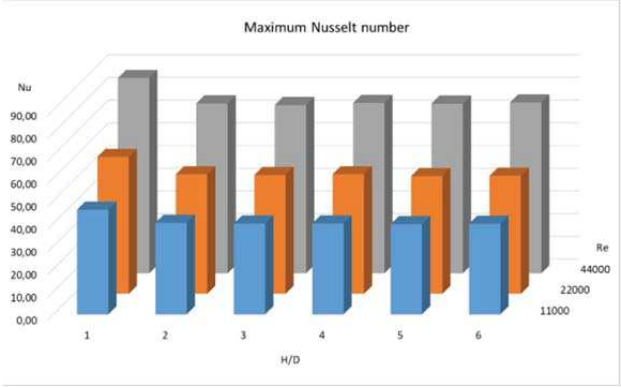

Fig. 10. Column graph showing Nusselt number for each configuration

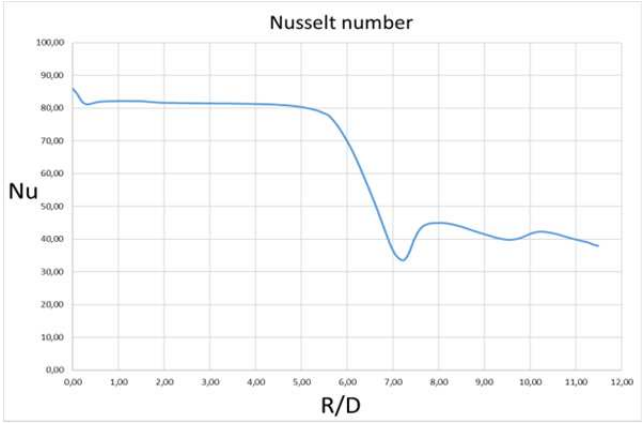

Fig. 11. Graph of Nusselt number values on the top side of the sample from the center to the outlet, for Re= 44000 and H/D= 1

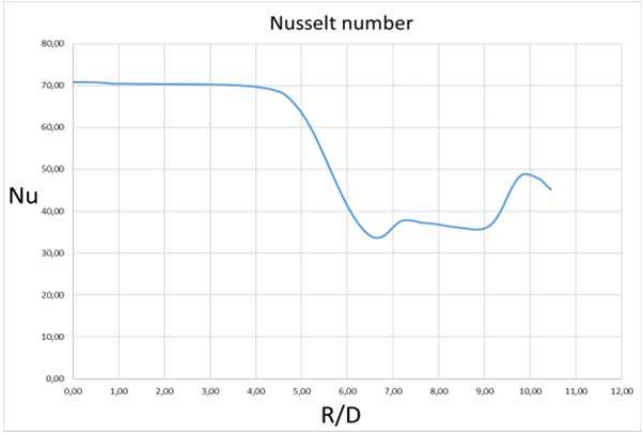

Fig. 12. Graph of Nusselt number values on the top side of the sample from the center to the outlet, for Re= 44000 and H/D= 3

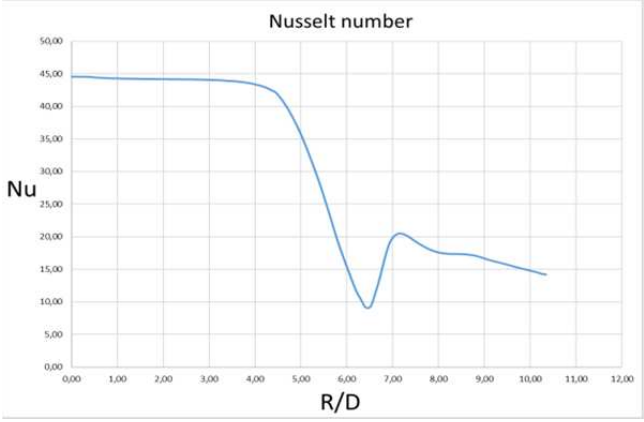

Fig. 13. Graph of Nusselt number values on the top side of the sample from the center to the outlet, for Re= 11000 and H/D= 1

Figures 11-13 present that the highest value of the Nusselt number is located in the center of stagnation region. Further to the outlet between R/D 0,5:5 (depending on the configuration) high Nusselt numbers are obtained due to the high-speed flow region over the wall, which influences heat transfer. When the flow speed over the cooled wall drops due to viscosity forces, the same does Nusslet number.

3.2. Results of double nozzle 3D simulation

Results obtained from double nozzle configuration shows different dependency of heat transfer parameters from geometrical configurations. The best average heat transfer coefficient was achieved for the largest distance between nozzles and cooled surface: S/D=4 an H/D=6 (Fig. 14).

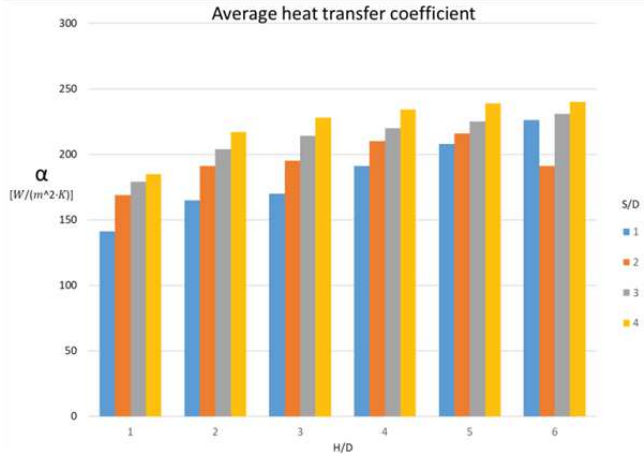

Fig. 14. Bar graph of average heat transfer depending on S/D and H/D

The larger the distance between nozzles themselves and cooled surface the better average heat transfer, this tendency is caused by minimizing the bigger distance interaction between flows coming from nozzle outlet. Each nozzle for S/D=4 an H/D=6 has its cooling area whereas with smaller distances as in S/D=1 (Figs. 15, 16) interaction between flows enable to create such separate cooling areas.

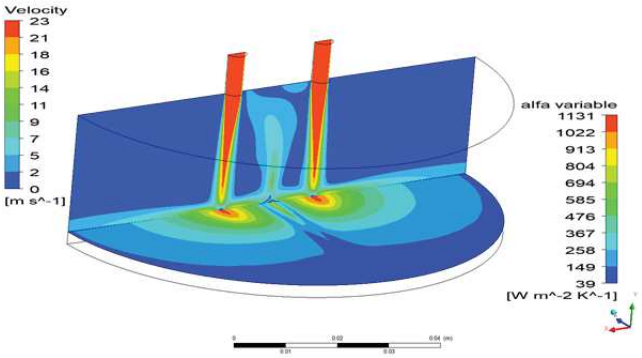

Fig. 15. Velocity (vertical) and heat transfer coefficient (horizontal) contours for H/D=6 and S/D=4

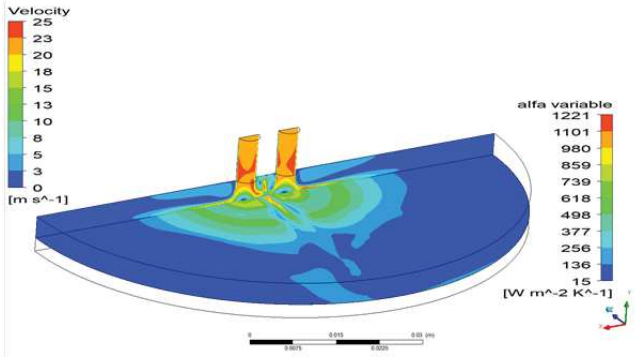

Fig. 16. Velocity (vertical) and heat transfer coefficient (horizontal) contours for H/D=6 and S/D=4

4. Conclusions

The 2D model calculations carried out indicated that the Reynolds number influences the most average heat transfer coefficient and Nusselt number. On the basis of the results obtained, the *D/H=1, Re=44000* set of parameters was considered the most optimal configuration.

The results of the 2D simulation obtained suggest that the nozzle to nozzle and nozzle to surface distance is significant for the detail cooling uniformity and cooling properties of the whole manifold. A non-uniform distribution of temperature during the time when the martensitic transformation takes place is undesirable since it results in an appearance of quenching distortions.

The graphs made on the basis of the results obtained during the simulations conducted suggest that the flow field strongly influences heat transfer between the fluid and solid domain. Double nozzle configuration has totally different flow structure and patterns, comparing to single nozzle configuration. Thus it has also different heat transfer parameters and their optimum depending on the geometrical configuration. The flows from neighboring nozzles affect each other before their reach cooling surface. This influence depends on the nozzle mutual location, bigger or smaller number of active nozzles and the layout thereof. As the intuition would suggest, the smaller distance between the nozzles, the more they affect each other, resulting in worse heat transfer from the cooling surface. With the increase of the distance between the nozzles better heat transfer coefficient distribution on the cooling surface accrues. The best average HTC was obtained for H/D=6 and S/D=4.

Simulations show that regarding considering the manifold of the nozzle, there is a need for more holistic approach. Single nozzle flow and heat transfer differ from the double configuration.

Acknowledgements

The research and publication were financed by the National Centre for Research and Development as part of the project no. POIR.04.01.04-00-0087/15 entitled: "Equipment for high performance and precise heat treatment with a quenching deformation reduction system for direct application in downstream production chains of mechanical gearing and bearings."

References

[1] D. Herring, Understanding Component Failures. Part 1: Mechanisms. Analysis Methods, Industrial Heating 7-8 (2013) 16-18.
[2] D. Wulpi, Understanding How Components Fail, ASM International, Materials Park, 2013.
[3] K. Dybowski, J. Sawicki, P. Kula, B. Januszewicz, R. Atraszkiewicz, S. Lipa, The effect of the quenching method on the deformations size of gear wheels

after vacuum carburizing, Archives of Metallurgy and Materials 61/2B (2016) 1057-1062, doi: https://doi.org/10.1515/amm-2016-0178.
[4] B.W. Kruszyński, Z. Gawroński, J. Sawicki, P. Zgórniak, Enhancement of gears fatigue properties by modern termo-chemical treatment and griding processes, Mechanics and Mechanical Engineering 12/4 (2008) 387-395.
[5] Z. Gawroński, J. Sawicki, Technological surface layer selection for small module pitches of gear wheels working under cyclic contact loads, Materials Science Forum 513 (2006) 69-74, doi: https://doi.org/10.4028/www.scientific.net/MSF.513.69.
[6] M. Korecki, E. Wołowiec-Korecka, M. Sut, A. Brewka, W. Stachurski, P. Zgórniak, Precision case hardening by low pressure carburizing (LPC) for high volume production, HTM – Journal of Heat Treatment and Materials 72/3 (2017) 175-183, doi: https://doi.org/10.3139/105.110325.
[7] Z. Gawroński, A. Malasiński, J. Sawicki, A selection of the protective atmosphere eliminating the inter-operational copper plating step in the processing of gear wheels, Archives of Materials Science and Engineering 44/1 (2010) 51-57.
[8] M. Korecki, E. Wołowiec-Korecka, D. Glenn, Single-piece, high-volume, low-distortion case hardening of gears, Proceeding of the AGMA Fall Technical Meeting, Detroit, USA, 2015.
[9] M. Korecki, E. Wołowiec-Korecka, In-line, high-volume, low-distortion, precision case hardening for automotive, transmission and bearing industry, Proceedings of the 23rd International Congress of Advanced Thermal Processing, Savanah, USA, 2016, 71-77.
[10] M. Korecki, E. Wołowiec-Korecka, A. Brewka, Unicase Master – In-line, high-volume, low-distortion, precision case hardening for automotive, transmission and bearing industry, Proceedings of the 3rd International Conference on Heat Treatment and Surface Engineering in Automotive Applications, Prague, Czech Republic, 2016.
[11] M. Korecki, E. Wołowiec-Korecka, D. Glenn, Single-piece, high-volume, low-distortion case hardening of gears, Thermal Processing 9/10 (2016) 32-39.
[12] E. Wołowiec-Korecka, M. Korecki, W. Stachurski, P. Zgórniak, J. Sawicki, A. Brewka, M. Sut, M. Bazel, System of single-piece flow case hardening for high volume production, Archives of Materials Science and Engineering 79/1 (2016) 37-44, doi: 10.5604/18972764.1227661.
[13] N. Zuckerman, N. Lior, Jet impingement heat transfer: Physics, correlations, and numerical modeling, Advances in Heat Transfer 39 (2006) 565-631, doi: https://doi.org/10.1016/S0065-2717(06)39006-5.
[14] R.J. Goldstein, K.A. Sobolik, W.S. Seol, Effect of Entrainment on the Heat Transfer to a Heated Circular Air Jet Impinging on a Flat Surface, Journal of Heat Transfer 112/3 (1990) 608-611, doi: 10.1115/1.2910430.
[15] L. Huang, M.S. El-Genkt, Heat transfer of an impinging jet on a flat surface, International Journal of Heat and Mass Transfer 37/13 (1994) 1915-1923, doi: https://doi.org/10.1016/0017-9310(94)90331-X.
[16] M. Behnia, S. Parneix, Y. Shabany, P.A. Durbin, Numerical study of turbulent heat transfer in confined and unconfined impinging jets, International Journal of Heat and Fluid Flow 20/1 (1999) 1-9, doi: https://doi.org/10.1016/S0142-727X(98)10040-1.
[17] K. Jambunathan, E. Lai, M.A. Moss, B.L. Button, A review of heat transfer data for single circular jet impingement, International Journal of Heat and Fluid Flow 13/2 (1992) 106-115, doi: https://doi.org/10.1016/0142-727X(92)90017-4.
[18] M.V. Jensen, J.H. Walther, Numerical Analysis of Jet Impingement Heat Transfer at High Jet Reynolds Number and Large Temperature Difference, Heat Transfer Engineering 34/10 (2013) 801-809, doi: https://doi.org/10.1080/01457632.2012.746153.
[19] Y. Shi, A.S. Mujumdar, M.B. Ray, Effect of large temperature difference on inpingement heat transfer under a round turbulent jet, International Communications in Heat and Mass Transfer 31/2 (2004) 251-260, doi: 10.1016/S0735-1933(03)00230-6.
[20] Y. Shi, M.B. Ray, A.S. Mujumdar, Effect of Large Temperature Differences on Local Nusselt Number Under Turbulent Slot Impingement Jet, Drying Technology 20/9 (2002) 1803-1825, doi: https://doi.org/10.1081/DRT-120015415.
[21] Y. Shi, M.B. Ray, A.S. Mujumdar, Computational Study of Impingement Heat Transfer under a Turbulent Slot Jet, Industrial and Engineering Chemistry Research 41/18 (2002) 4643-4651, doi: 10.1021/ie020120a.
[22] P. Heikkilä, N. Milosavljevic, Investigation of Impingement Heat Transfer Coefficient At High Temperatures, Drying Technology 20/1 (2002) 211-222, doi: https://doi.org/10.1081/DRT-120001375.
[23] H. Martin, Heat and Mass Transfer between Impinging Gas Jets and Solid Surfaces, Advances

in Heat Transfer 13 (1977) 1-60, doi: https://doi.org/10.1016/S0065-2717(08)70221-1.

[24] R. Viskanta, Heat Transfer to Impinging Isothermal Gas and Flame Jets, Experimental Thermal and Fluid Science 6/2 (1993) 111-134, doi: https://doi.org/10.1016/0894-1777(93)90022-B.

[25] C. Wan, Y. Rao, P. Chen, Numerical predictions of jet impingement heat transfer on square pin-fin roughened plates, Applied Thermal Engineering 80 (2015) 301-309, doi: https://doi.org/10.1016/j.applthermaleng.2015.01.053.